Applied Catalysis B: Environmental 300 (2022) 120750

Contents lists available at ScienceDirect

Applied Catalysis B: Environmental

journal homepage: www.elsevier.com/locate/apcatb

Covalent grafting of cobalt aminoporphyrin-based electrocatalyst onto carbon nanotubes for excellent activity in CO_2 reduction

Shengshen Gu, Aleksei N. Marianov, Yijiao Jiang *

School of Engineering, Macquarie University, Sydney, NSW 2109, Australia

ARTICLE INFO

Keywords:
Covalent immobilization
Cobalt porphyrins
Carbon nanotubes
CO_2 electroreduction
In-situ spectroscopy

ABSTRACT

Electrochemical reduction of carbon dioxide (CO_2ERR) provides a promising method for managing global carbon balance by transforming CO_2 into green chemicals. However, the development of efficient electrocatalysts for the fast and selective CO_2 reduction is still a big challenge. Herein we report a study on CO_2ERR electrocatalytic activity of amino-substituted Co porphyrin (CoTAP) as a function of its immobilization mode. It is demonstrated that the covalently grafted complex CoTAP-cov exhibits a turnover frequency to CO formation (TOFco) of 6.0 s^{-1} and the Faradic efficiency to CO (FEco) of ~100% at the overpotential of 550 mV making it one of the best catalysts to date. In contrast, noncovalently immobilized counterpart CoTAP-noncov shows a more moderate TOFco of 2.3 s^{-1} and lower FEco of 85%. Our results demonstrate that the presence of the donating -NH_2 groups within the lateral aromatic moiety is required to maximize the activity of the complex in CO_2ERR. In turn, covalent grafting both mitigates the aggregation of the porphyrin catalyst and enhances the interfacial electron delivery rate. The combination of these factors furnishes a catalyst with an excellent intrinsic TOFco as high as 36.6 s^{-1}.

1. Introduction

Electrochemical reduction of CO_2 (CO_2ERR) has been extensively studied as a process that could produce value-added chemicals from CO_2 in an aqueous solution [1]. Numerous heterogeneous electrocatalysts driving CO_2ERR have been developed ranging from transition metals [2–4] and carbonaceous composites [5,6] to molecular complexes [7–9]. Among them, porphyrins with non-noble metal centers draw increasing attention due to their capability to selectively reduce CO_2 to CO, which in turn can be further processed into liquid fuels via Fischer-Tropsch synthesis [10]. However, both activity and selectivity of these complexes need to be further enhanced to make them viable for potential industrial applications.

Generally, two complimentary approaches to improve the performance of a molecular catalyst might be conceived. In the first method, modification of the molecular structure could be used to tune the distribution of the electron density which leads to a higher intrinsic activity. Indeed, it was reported that the donating groups increase the partial negative charge on the metal center via inductive effect. This results in higher CO_2-to-metal binding energy and thus enhanced activity in CO_2ERR [11]. Amino group (-NH_2) is one of such groups that has high electronegativity. Indeed, Co tetraphenylporphyrin exhibits an improved performance in CO_2 reduction to CO compared to the unsubstituted analogue [12]. However, the latter study was conducted in organic electrolyte which is undesirable for future applications due to the problem of catalyst recycling.

A second method that could furnish a better catalyst relies on careful optimization of the catalytically active layer morphology. In this regard, the choice of the immobilization technique proved to be one of the decisive factors affecting both catalyst turnover frequency (TOFco) and the Faradic efficiency to CO (FEco). Several approaches have been employed to immobilize porphyrins on the electrode surface. One of them is based on non-covalent binding of porphyrins to the carbonaceous supports via π-π interactions [13]. For example, pyrene-appended Fe porphyrin was immobilized on carbon nanotubes (CNTs) and a turnover number (TON) of 813 was achieved at an overpotential of 480 mV after a 12 h electrocatalysis [14]. Cobalt chlorin was also immobilized on CNTs and a FEco of 89% was achieved at 510 mV overpotential [15]. Another strategy for the immobilization of the porphyrins employs coordination of the metal centers to the functional groups on the surface-modified electrodes [16]. In this regard, the cobalt porphyrins were chemically adsorbed onto pyridine-modified glassy carbon via

* Corresponding author.
E-mail address: yijiao.jiang@mq.edu.au (Y. Jiang).

https://doi.org/10.1016/j.apcatb.2021.120750
Received 22 July 2021; Received in revised form 27 August 2021; Accepted 22 September 2021
Available online 24 September 2021

coordination and an enhanced activity was achieved [17–19]. More recently, our group has also immobilized cobalt tetraphenyl porphyrin (CoTPP) on TiO_2 nanotubes in a coordinating environment provided by pyridine [20].

However, the above-mentioned cases adopt noncovalent immobilization which may lead to slow electron transfer and weak connection to the support [21–23]. Indeed, an inferior catalytic activity of the noncovalently immobilized porphyrin in CO_2ERR was reported previously [20]. In contrast, covalent immobilization is quite promising since a strong chemical bond is formed between the catalyst and the support which results in an improved activity. For instance, our group has covalently tethered CoTPP to carbon cloth via phenylene link using in situ electroreduction of the corresponding diazonium salt [24]. An enhanced catalytic activity was achieved with the total CO production 2.5 times higher than the noncovalent counterpart after a 4 h electrocatalysis. However, the performance is yet to meet the industrial requirements owing to the relatively modest intrinsic activity of CoTPP. Also, the use of diazonium salts for the modification of powder-like CNTs requires a large excess of expensive porphyrin substrate [25], and a more atom-efficient method would be beneficial.

Thus, we endeavoured to combine the benefits of both approaches mentioned above by immobilizing covalently a porphyrin-based catalyst bearing donating substituents onto the surface of multiwalled CNTs. Co tetrakis-(4-aminophenyl) porphyrin (CoTAP) was chosen as a catalyst and its covalent grafting was achieved via nucleophilic substitution of Cl^- within the in-situ generated -COCl modified CNTs. The properties of the resulting composite were studied using Raman and FTIR spectroscopies, TEM imaging, and a range of electrochemical methods. The activity of covalently grafted CoTAP was studied by cyclic voltammetry (CV) and controlled potential electrolysis. In-situ spectroelectrochemical measurements were performed to monitor the evolution of the active sites under the real working conditions.

2. Experimental

2.1. Chemicals

All chemicals were purchased from Sigma Aldrich. Multi-walled carbon nanotubes (carboxylic acid functionalized, CNTs) were used as received. Pyrrole was distilled under reduced pressure prior to use. Carbon fibre paper was purchased from the Fuel Cell Store. The synthesis of CoTAP is detailed in the Supporting Information (SI).

2.2. Preparation of CoTAP-cov and CoTAP-noncov

CoTAP-noncov: 2 mg of CNTs and 10 μL of 5% Nafion were dispersed in 1 mL isopropanol by 30 min sonication to form ink I. CoTAP was dissolved in DMF to form ink II. A predetermined volume of ink II was mixed with 60 μL ink I to ensure a fixed amount of CNTs with a variety of CoTAP loadings (specified in Table S1). The mixed ink was further sonicated for 30 min and drop casted on each side of 1 cm^2 carbon fibre paper. The afforded electrode was dried in an oven at 80 ℃.

CoTAP-cov: CoTAP was covalently ligated to CNTs via an amide bond to afford modified CNTs (CoTAP-cov) according to the literature [26]. The preparation method is detailed in the SI. The cobalt content was determined to be 0.21 wt% by microwave plasma-atomic emission spectrometer (MP-AES). Then 2 mg of CoTAP-cov and 10 μL of 5% Nafion were dispersed in 1 mL of isopropanol by a 30 min sonication to form ink III. 60 μL of ink III was drop casted on each side of the 1 cm^2 piece of carbon fibre paper and left to dry in an oven at 80 ℃. The surface concentration of CoTAP was calculated to be 4×10^{-9} mol/cm^2. For the study involving the variation of surface concentration, different volumes of ink III were mixed with ink I (2 mg/mL CNTs) for drop casting (specified in Table S2). It should be noted that the amount of CNTs for CoTAP-cov is the same as for CoTAP-noncov at ~120 $\mu g/cm^2$.

2.3. Electrochemical studies

All electrochemical measurements were conducted on BioLogic SP-300 potentiostat with 85% *iR* compensation at room temperature of 23 °C. Ag/AgCl (3.5 M KCl) was used as a reference electrode and a platinum foil was employed as a counter electrode. 0.5 M $KHCO_3$ was used as the aqueous electrolyte. All potentials in this study are referenced to Ag/AgCl (−0.205 V vs NHE).

Cyclic voltammetry (CV) was performed in a single compartment cell with aqueous electrolyte at a scan rate of 100 mV/s. The cell was purged with Ar or CO_2 prior to the tests. The long-run electrolyses were performed in an H-cell shielded from light with a Nafion-117 membrane as a separator. The two compartments were filled with aqueous electrolyte and purged with CO_2 for 30 min prior to the long-run electrolysis. The stability of CoTAP-cov and CoTAP-noncov in CO_2ERR was studied using a 24 h long electrolysis under the potential of − 1.30 V (−1.095 V vs NHE) in 0.5 M $KHCO_3$ under continuous CO_2 flow of 5 mL/min through the cathodic compartment. The quantitative assessment of the stability was based on the law of the first order kinetics (description is provided in the SI). The gaseous products from cathodic compartment were analyzed on a Shimadzu gas chromatograph GC-2014 equipped with a MolSieve 5 A packed column and a thermal conductivity detector (TCD) using ultrapure helium carrier gas (99.9999%).

2.4. Material characterization

The attenuated total reflection infrared (ATR-IR) spectroscopy was conducted on Thermo Scientific Nicolet 6700 spectrometer with a deuterated triglycine sulphate (DTGS) detector. The Raman spectra were collected using a confocal LabRAM HR Evolution instrument (Horiba) equipped with a visible 633 nm laser and a high-grade Leica microscope. In-situ Raman study was performed under the same conditions in a custom-made cell filled with CO_2-saturated 0.5 M $KHCO_3$ and a Nafion membrane separating the cathodic and anodic chambers. Transmission electron microscope (TEM) images were obtained on Philips CM10 TEM at 100 kV. UV–vis spectra were collected on Jinghua UV1800PC. Catalyst before and after electrolysis were dispersed in DMF for acquiring UV–vis spectra. In-situ UV–vis spectroscopy was performed on Jinghua UV1800PC using a 5 mL quartz cuvette as a one-compartment electrochemical cell. The cell was filled with 0.5 M $KHCO_3$ saturated with CO_2. Fluorine-doped tin oxide (FTO) glass with CoTAP drop casted on the surface was used as the working electrode. To assure the equilibration of the system the FTO electrode was held at the chosen potentials for 2 min before acquiring a spectrum.

3. Results and discussion

3.1. Catalyst synthesis and characterization

The synthesis of covalently immobilized CoTAP (CoTAP-cov) was performed in two stages as illustrated in Fig. 1. First, CNTs were activated by converting the surface -COOH moieties into the -COCl groups using a 24 h reflux in $SOCl_2$. Thus formed -COCl modified CNTs were treated with the solution of CoTAP furnishing the final composite CoTAP-cov. The content of CoTAP in the resulting material was determined to be 0.21 wt% using microwave plasma-atomic emission spectroscopy (MP-AES). The electrodes were then manufactured via drop-casting of the ink containing CoTAP-cov onto the surface of carbon fibre paper to the CoTAP concentration of 4×10^{-9} mol/cm^2. Noncovalently immobilized counterpart CoTAP-noncov was prepared via drop casting of the ink consisting of CoTAP and CNTs. To assure the same amount of the catalyst is present in both materials, the CoTAP loading amount of 4×10^{-9} mol/cm^2 was used both for CoTAP-noncov and CoTAP-cov if not otherwise specified.

To determine the dispersion of CoTAP on the surface of CNTs, the resulting materials were studied using transmission electron microscopy

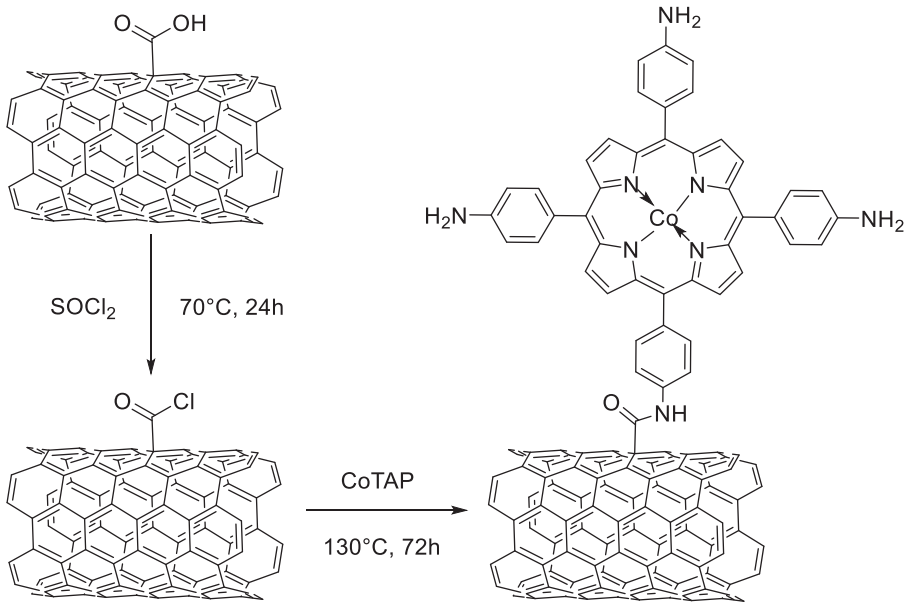

Fig. 1. Covalent ligation of CoTAP on CNTs (CoTAP-cov).

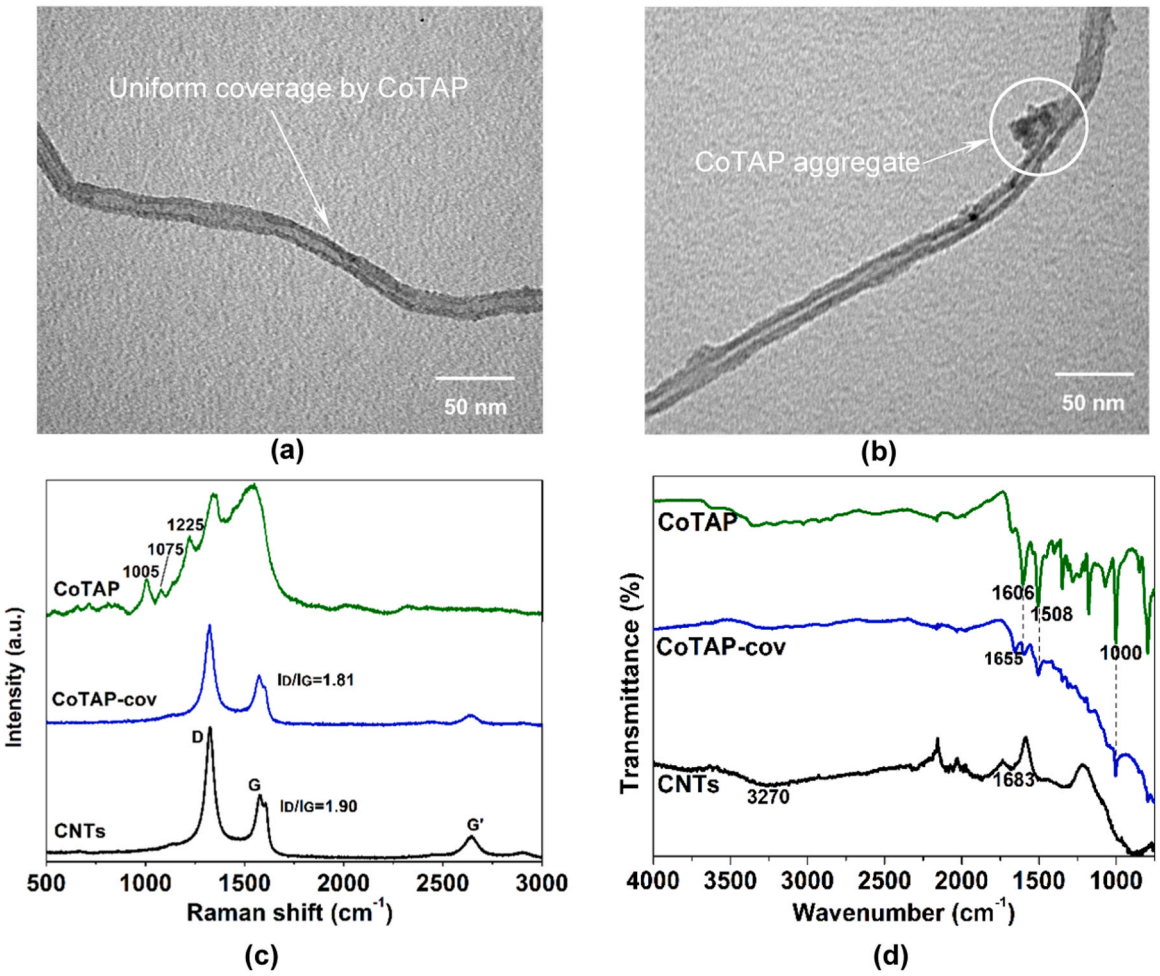

Fig. 2. Representative TEM images of (a) CoTAP-cov (4×10^{-9} mol/cm^2) and (b) CoTAP-noncov (4×10^{-9} mol/cm^2); (c) Raman and (d) FTIR spectra of CNTs (black line), CoTAP (green line) and CoTAP-cov (blue line). (For interpretation of the references to colour in this figure legend, the reader is referred to the web version of this article.)

(TEM) (Fig. 2a and b, S5a-b). As expected, TEM image of CoTAP-cov shows a uniform surface coverage with no noticeable aggregation (Fig. 2a, S5a). In contrast, noncovalently immobilized composite CoTAP-noncov features strong aggregation at the loading of 4×10^{-9} mol/cm^2 (Fig. 2b, S5b) which becomes even more pronounced at higher surface concentrations of 4×10^{-8} mol/cm^2 (Fig. S4). Hence, covalent immobilization helps to mitigate the formation of CoTAP clusters on the surface of CNTs.

Next, Raman spectroscopy was employed to gain more insights into the structure of the materials. As shown in Fig. 2(c), both CoTAP-cov and CNTs (carboxylic acid functionalized) display a prominent D band at ~1300 cm^{-1}, a G band at ~1500 cm^{-1} and a less intensive G′ band at ~2600 cm^{-1} as an overtone of D band [27]. The presence of these signals clearly shows that the structure of nanotubes remains intact upon covalent immobilization. However, the intensity ratio (I_D/I_G) measured for CoTAP-cov is 1.81 (Fig. 2c, blue trace), which is slightly lower than the ratio of $I_D/I_G = 1.90$ determined for CNTs (Fig. 2c, black trace). A similar change of I_D/I_G ratio upon introduction of covalently bound organic groups was reported earlier [26,28,29], indicating the successful grafting of the porphyrin complex on the surface. Interestingly, the peaks corresponding to the pure CoTAP [30,31] (Fig. 2c, blue trace) were not clearly observed in the spectrum of CoTAP-cov, most likely due to the low loading of complex. In covalent immobilization mode, the loading amount of CoTAP is limited by the number of anchoring group -COOH on CNTs.

The presence of the amide link was established using FTIR spectroscopy (Fig. 2d). CNTs show a characteristic broad peak at 3270 cm^{-1}, which is attributed to the O-H vibration. The peak at 1683 cm^{-1} is attributed to C═O stretching frequency of carboxyl moieties (-COOH). Whereas this peak shifted to 1655 cm^{-1} in CoTAP-cov due to the formation of amide bond (-CONH). A sharp peak corresponding to the skeletal ring vibration of the porphyrin macrocycle evolves at 1000 cm^{-1} in CoTAP, and similarly the same peak shows up in CoTAP-cov. Besides, another two peaks appeared in CoTAP attributed to the bending vibration of NH_2 (1508 cm^{-1}) and stretching vibration of C═C (1606 cm^{-1}) [26] were clearly observed in CoTAP-cov as well. These observations indicate that CoTAP was successfully immobilized on CNTs. To further confirm if CoTAP was covalently immobilized, we washed CoTAP-cov and CoTAP-noncov with copious amounts of solvent and compared their IR spectra (Fig. S6). After washing, the spectrum of CoTAP-noncov (Fig. S6) is the same as that of pristine CNTs (Fig. 2d), which implies that CoTAP was physically adsorbed on CNTs and can be easily washed off. On the other hand, the spectrum of CoTAP-cov shows negligible difference before and after washing (Fig. S6 and Fig. 2d) with all characteristic peaks still exist at 1655, 1606, 1508 and 1000 cm^{-1}, indicating that CoTAP was grafted to CNTs via a covalent bond.

Finally, the electrochemical behaviour and the amount of electrochemically active catalyst Γ_{EA} (mol/cm^2) were determined for both materials using CV in the degassed 1 M KOH electrolyte at the scan rates between 100 mV/s and 500 mV/s (Fig. 3a and b). Both electrodes feature a well-resolved reversible redox response of $Co^{II}TAP/[Co^{I}TAP]^-$ transformation at −1.05 V which unambiguously proves the successful immobilization of the organometallic catalyst on CNTs. Further, a linear dependence of peak current densities on the scan rates was observed for both CoTAP-noncov and CoTAP-cov (Fig. 3c and d), which indicates that CoTAP behaves as a heterogeneous catalyst. The respective Γ_{EA} values

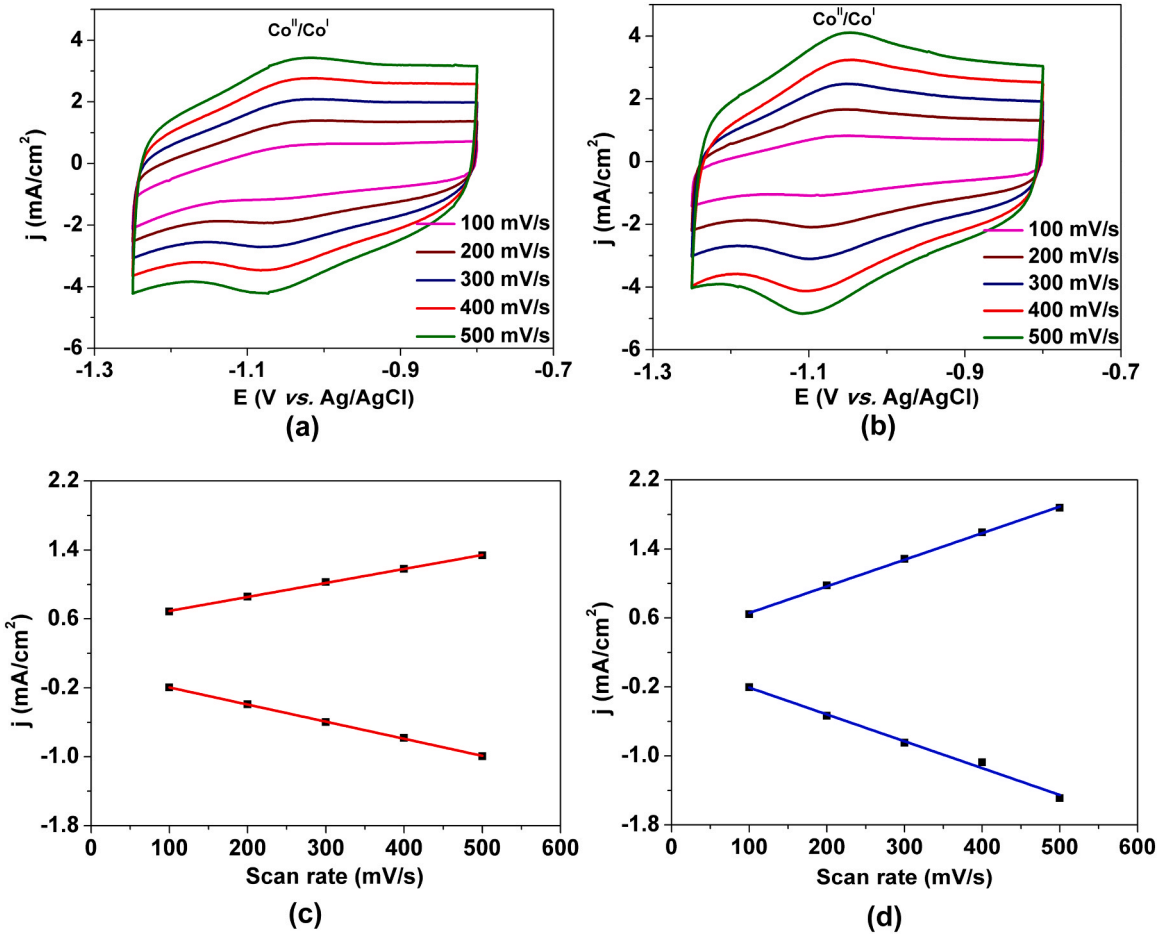

Fig. 3. CV of (a) CoTAP-noncov (4×10^{-9} mol/cm^2) (b) CoTAP-cov (4×10^{-9} mol/cm^2) in Ar-saturated 1 M KOH electrolyte at different scan rates; Dependence of peak current density at Co^{II}/Co^{I} on the scan rates for (c) CoTAP-noncov (d) CoTAP-cov.

were also determined via integration of the cathodic waves. In this regard, a stark difference was observed between immobilization methods. As such, CoTAP-noncov displays Γ_{EA} of 1.9×10^{-9} mol/cm^2 which constitutes only 48% of all surface-bound complex. In contrast, $\Gamma_{EA} = 3.5 \times 10^{-9}$ mol/cm^2 was measured for CoTAP-cov which means that at least 88% of the CoTAP was involved in the fast electron transfer process.

The observations described above provide important insights into the nature of the electrode materials. First of all, the CoTAP-cov features a strong amide bond between the porphyrin core and the surface of CNTs. Indeed, characteristic changes in the FTIR and Raman spectra coupled with the resistance of the material to the solvents confirm the presence of the direct amide link with the CNTs. Furthermore, the covalent connection with the conductive support allows for more efficient charge transfer onto the CoTAP within CoTAP-cov compared to CoTAP-noncov. The latter finding suggests significantly higher density of interfacial electron flux for covalently immobilized CoTAP-cov which could play a crucial role in the catalytic process. The chosen method of covalent immobilization also preserves 75% of -NH_2 groups which is a significant advantage compared to diazonium chemistry that leads to decomposition of all amino moieties [25].

3.2. Electrocatalytic activity

Encouraged by the results of characterization we embarked on the study of the electrocatalytic activity. To assess the overall performance, CV study in Ar- and CO_2-saturated 0.5 M $KHCO_3$ was performed first (Fig. 4a). The characteristic increase of the reductive current and a positive shift of the onset potential upon saturation with CO_2 were clearly observed. As measured at 2 mA/cm^2 current density, upon changing from Ar to CO_2, the potential shifted from −1.20 V to −1.08 V for CoTAP-cov (Fig. 4a, blue lines) and from −1.17 V to −1.08 V for CoTAP-noncov (Fig. 4a, red lines), indicating that both catalysts are more sensitive towards CO_2ERR. It was further noticed that upon transition from Ar to CO_2-saturated electrolyte, CoTAP-cov displays 25.4 mA/cm^2 increase of the current density while CoTAP-noncov exhibits a more moderate change of 13.4 mA/cm^2 (as measured at −1.35 V). It is known that the CV current is dominated by H_2 evolution reaction under Ar while CO_2ERR is the main contributor under CO_2. Thus, a greater change of the reductive current upon transition to CO_2-saturated electrolyte indicates that CoTAP-cov not only has a better activity towards CO_2 reduction, but also inhibits competitive H_2 evolution more efficiently. Hence, the CV clearly indicates that the CoTAP-cov is both more selective and active than its noncovalent counterpart.

Fig. 4(b) further shows the CV traces recorded for CoTAP-noncov at various loading amounts. The reduction current at −1.35 V rises with the CoTAP loadings in the range between 2×10^{-11} mol/cm^2 and 4×10^{-9} mol/cm^2. However, further increase of the surface loading to 2×10^{-8} mol/cm^2 and above does not improve the catalytic current, thus implying the saturation of CNTs surface at high loadings. Thus, the highest activity of CoTAP-noncov is achieved at the surface concentration of 4×10^{-9} mol/cm^2.

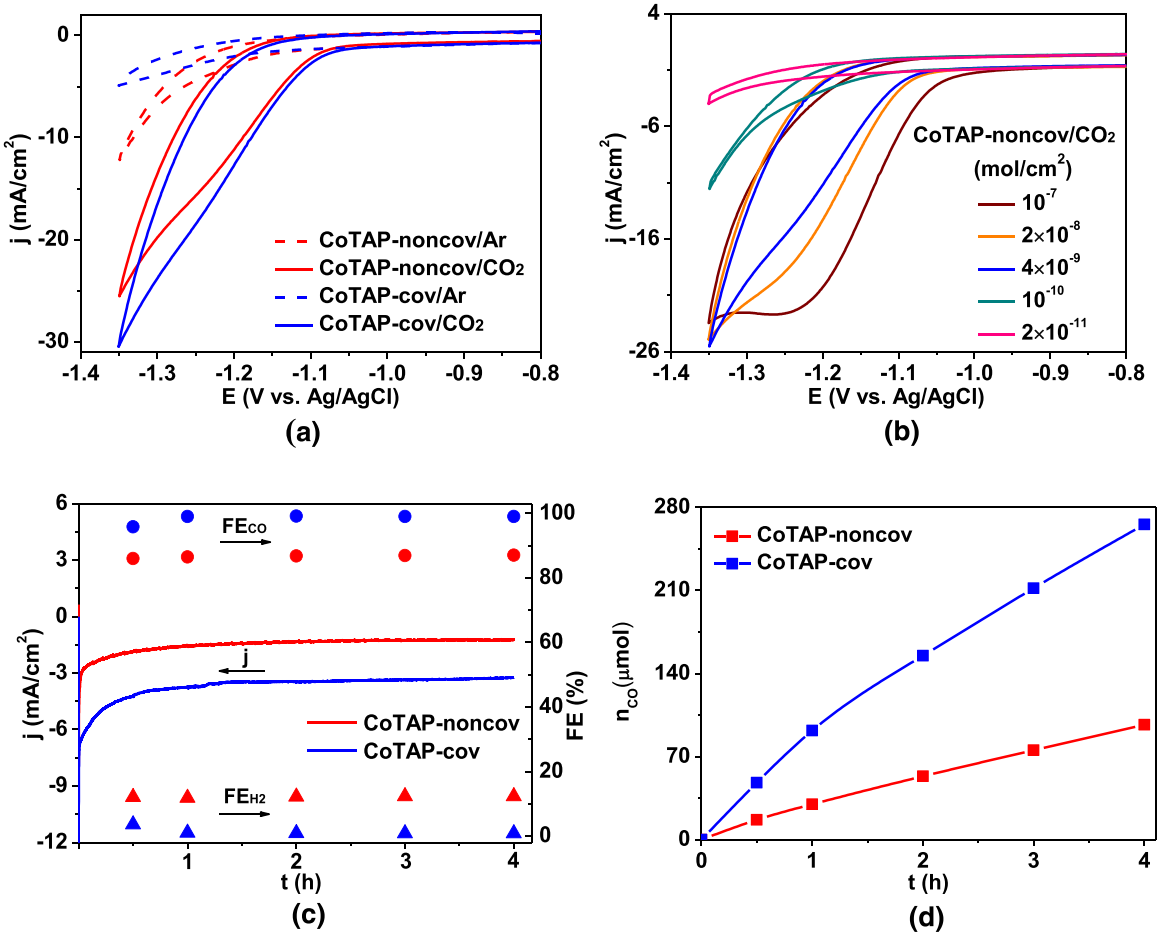

Fig. 4. (a) CV of CoTAP-noncov (4×10^{-9} mol/cm^2, red trace) and CoTAP-cov (4×10^{-9} mol/cm^2, blue trace) in Ar- and CO_2-saturated aqueous electrolyte; (b) CV of CoTAP-noncov at various loading amounts in CO_2-saturated electrolyte. (scan rate: 100 mV/s, aqueous electrolyte: 0.5 M $KHCO_3$); (c) current density, FEco and (d) CO production observed on CoTAP-noncov and CoTAP-cov during a 4-h long electrolysis at −1.30 V (−1.095 V vs NHE, η = 565 mV). Electrolyte: 0.5 M $KHCO_3$ in all cases. (For interpretation of the references to colour in this figure legend, the reader is referred to the web version of this article.)

To confirm these findings, 4 h long electrolyses were conducted at −1.30 V (−1.095 V vs NHE, η = 565 mV). In full agreement with the CV, CoTAP-cov shows excellent FEco of nearly 100% and a steady current of ~ 4 mA/cm^2 during the entire process (Fig. 4c, blue traces). In total, 265 μmol CO was produced in 4 h (Fig. 4d, blue trace), which translates into a TONco of 6.6 × 10^4. In contrast, CoTAP-noncov shows a lower activity with the reductive current of ~2.5 mA/cm^2 and a moderate FEco of ~86% (Fig. 4c, red traces). This results in only 97 μmol of CO corresponding to TONco = 2.4 × 10^4 produced over the course of 4-h electrolysis (Fig. 4d, red trace). In a control experiment, bare -COOH modified CNTs were also subject to electrolysis under the identical conditions, i.e. at −1.30 V in CO_2-saturated $KHCO_3$. The non-activated CNTs were employed as a reference since -COCl groups are sensitive to the moisture and would yield -COOH modified CNTs upon exposure to the electrolyte [32]. No CO was detected, suggesting that CNTs are not active in CO_2ERR, and the reaction is driven only by CoTAP. It is important to note that the TON obtained on CoTAP-cov is 2.75 times higher than that on CoTAP-noncov, whereas its Γ_{EA}(CoTAP) is only 1.85 times larger. Thus, covalent grafting not only enhances the amount of the active catalyst (vide supra), but also improves its formal per-site turnover frequency (TOFco).

Next, we endeavoured to gain insight into the kinetics of CO_2ERR using a series of 60 min long electrolyses under the potentials between −1.20 and −1.40 V. As shown in Fig. 5(a), a maximum current density of 5.9 mA/cm^2 was sustained by CoTAP-cov at −1.40 V while CoTAP-noncov gives only 3.0 mA/cm^2 under the same conditions (Fig. 5b). As expected, CoTAP-cov exhibits an excellent activity across the entire potential range with the TOFco continuously rising from 2.7 s^{-1} at −1.20 V to 6.3 s^{-1} at −1.40 V (Fig. 5c, blue bars). For CoTAP-noncov, the TOFco is more moderate and ranges from 1.0 to 2.3 s^{-1} peaking at −1.35 V and declining to 2.0 s^{-1} at −1.40 V (Fig. 5c, red bars).

The reason behind the observed drop of TOF at high overpotentials for CoTAP-noncov becomes apparent when the respective FEco values are considered. Indeed, although at −1.30 V the noncovalently immobilized material exhibits FEco of 86%, it drops below 50% at −1.40 V which means that the majority of current is spent on H_2 evolution. While showing a similar trend, CoTAP-cov exhibits generally higher FEco with the minimum of 90% at −1.20 V and maximum of ~100% at-1.25 V and −1.30 V. It must be also noted that the peak FEco of ~100% was reached at −1.25 V for CoTAP-cov, which is 50 mV smaller overpotential compared to CoTAP-noncov which displays the maximum FEco at − 1.30 V. It is also notable that the structure of CoTAP-cov remains intact even at the potentials as negative as −1.40 V. The characteristic Soret and Q bands remain at the same position in the UV-Vis spectrum after 60 min electrolysis (Fig. S7). However, the intensity of the absorption bands decreases over the course of electrolysis. The latter phenomenon was observed for the other Co porphyrin-based catalysts [33] and ascribed to a slow transition of the catalyst into the Co^{III} state and reductive carboxylation [34].

Finally, to characterize the influence of the immobilization mode on the stability of both catalysts, 24 h electrolyses under continuous flow of CO_2 (5 mL/min) were conducted (Fig. 6a). The long-run CO_2ERR was performed at −1.30 V where the catalysts show the highest selectivity to CO. The CoTAP-cov sustains a stable FEco above 95% during the entire experiment (Fig. 6a, blue dots). In contrast, for CoTAP-noncov the FEco reaches 85% at the beginning of the experiment and drops below 80%

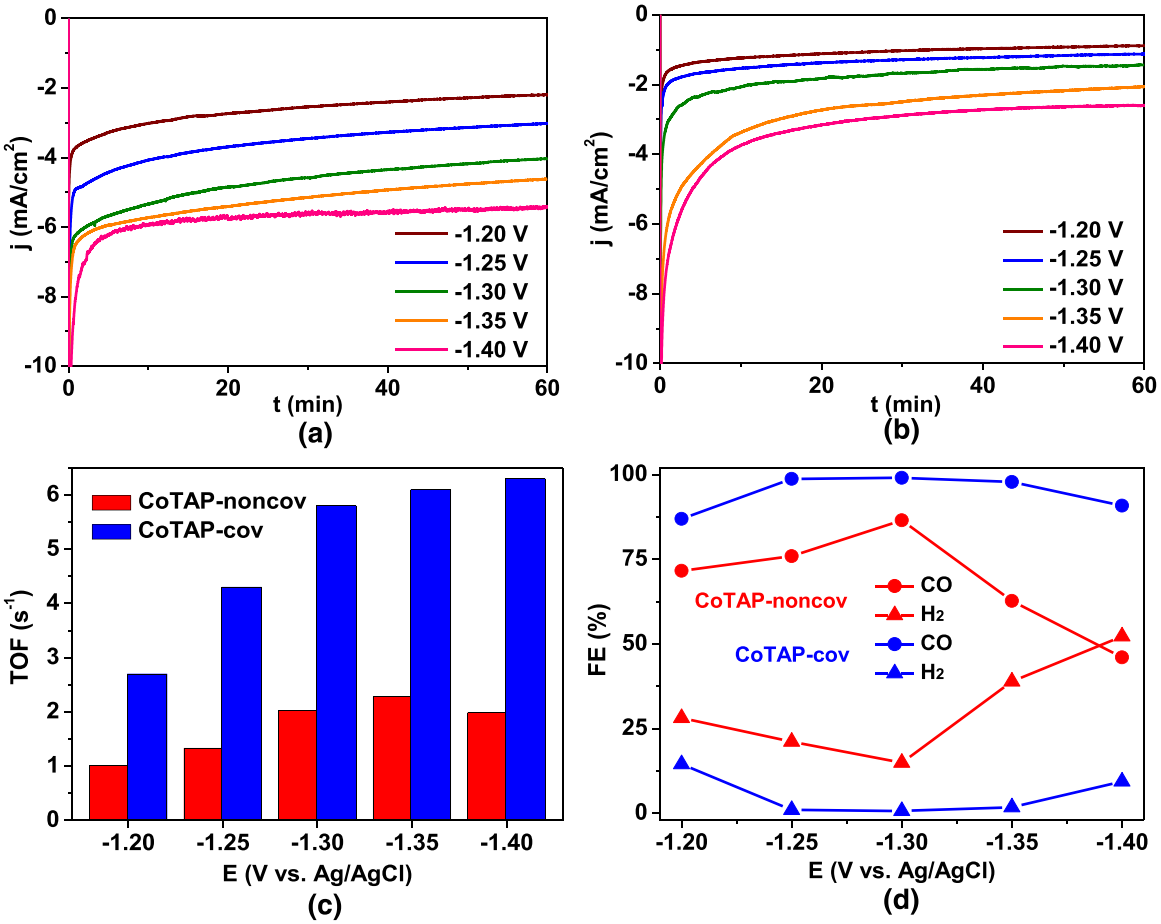

Fig. 5. Current densities observed during CO_2ERR on (a) CoTAP-cov (4 × 10^{-9} mol/cm^2) and (b) CoTAP-noncov (4 ×10^{-9} mol/cm^2); (c) TOFco and (d) FEco and FE_{H2} for CoTAP-noncov and CoTAP-cov recorded in a 60-min electrolysis under the potentials between −1.20 and −1.40 V. (For interpretation of the references to colour in this figure legend, the reader is referred to the web version of this article.)

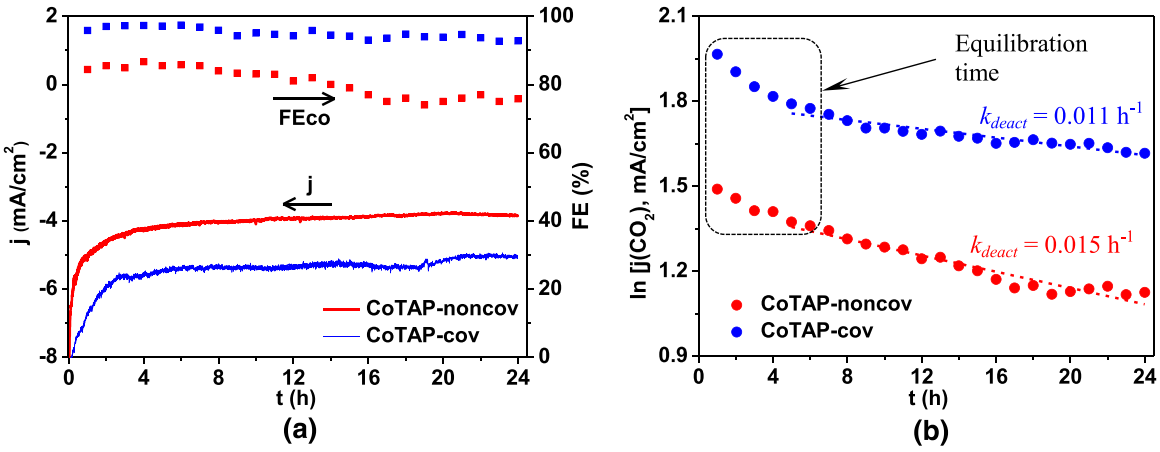

Fig. 6. (a) FEco, total current density and (b) logarithmic representation of CO_2ERR-specific current of CoTAP-cov (blue lines) and CoTAP-noncov (red lines) over 24 h long run. (For interpretation of the references to colour in this figure legend, the reader is referred to the web version of this article.)

after 13 h of electrolysis (Fig. 6a, red dots).

The quantitative characterization of the stability was achieved by deriving the kinetic constants of the deactivation k_{deact} from the current decay curves (Fig. 6a). As mentioned above, the CNTs are inactive in CO_2ERR, thus the CO_2ERR-specific current j(CO_2ERR) (mA/cm^2) is directly proportional to the surface concentration of the active CoTAP. To test if the loss of activity follows the first order kinetics, the natural logarithm of the CO_2ERR-specific current density j(CO_2) was plotted against the experiment time as shown in Fig. 6(b) [35]. Clearly, the resulting line show two major regions. First non-linear region lasting for the first 6 h could be attributed to the equilibration of the pH and CO_2 concentration throughout the bulk electrolyte [36]. However, after 6 h the process displays a well-defined linear j(CO_2ERR)-t correlation confirming the first order deactivation kinetics. The rate constants k_{deact} were obtained as the slope of the resulting linear relationships (Fig. 6b). In this regard, CoTAP-cov exhibits k_{deact} of 0.011 h^{-1} while CoTAP-noncov shows k_{deact} = 0.015 h^{-1}. These correspond to the characteristic catalyst half-lives $t_{1/2}$ of 63 h for CoTAP-cov and 46 h for CoTAP-noncov. Hence, the covalent immobilization not only improves the activity of the CoTAP, but also renders it to be 1.4 times more stable.

The performance of CoTAP-cov is quite remarkable as the catalyst shows one of the highest TOFco and FEco to date (Table 1). The activity and selectivity achieved in this work surpass by far the results reported for covalently and noncovalently immobilized Co porphyrins (Entries 4–11). This most likely could be attributed both to the presence of donating -NH_2 groups within CoTAP and direct connection to the surface of CNTs [11]. Indeed, the catalysts described in the Entries 4–10 do not contain donating substituents or immobilized noncovalently thus exhibiting generally lower TOFs. Only in the report referenced in Entry 3, the TOFco = 8.3 s^{-1} of covalently grafted CoTPP-cov surpasses the TOFco observed in this work. However, this is likely due to the TOFco calculation of Entry 3 being based on the Γ_{EA} value while the present result is derived from the total loading amount which is a lower limit of TOF. It must be also noted that both CoTAP-cov and CoTAP-noncov surpass the performance of Fe- (Entries 12–16) and Ni- (Entry 17) based porphyrins. This difference most likely stems from the generally higher activity of Co complexes in the aqueous electrolytes.

Table 1
Comparison of the reported porphyrin catalysts for electroreduction of CO_2 to CO in aqueous electrolyte.

Entry	Catalyst	V vs NHE	Electrolyte	FEco (%)	TOF (s^{-1})	Ref.
1	**CoTAP-cov**	-1.095	0.5 M $KHCO_3$	~100	6.0	This work
2	**CoTAP-noncov**	-1.095	0.5 M $KHCO_3$	86	2.0	This work
3	CoTPP-cov	-1.05	0.5 M $KHCO_3$	67	8.3	[24]
4	CoTPP-noncov	-1.05	0.5 M $KHCO_3$	52	4.5	[24]
5	CoTPP/CNT	-1.10	0.5 M $KHCO_3$	70	2.75	[33]
6	CoPP@CNT	-1.031	0.5 M $NaHCO_3$	98.3	1.9	[37]
7	COF-367-Co	-1.09	0.5 M $KHCO_3$	91	0.53	[38]
8	COF-367-Co (1%)	-1.09	0.5 M $KHCO_3$	53	2.6	[38]
9	CoCoPCP	-0.97	0.5 M $KHCO_3$	94	2.4	[39]
10	COF-366-$(OMe)_2$-Co@CNT	-1.10	0.5 M $KHCO_3$	94	1.2	[40]
11	CoTMAP	-0.99	0.5 M $NaHCO_3$	97.8	5.0	[11]
12	CAT_{CO2H}	-1.06	0.5 M $KHCO_3$	86	0.05	[41]
13	CAT_{pyr}/CNT	-1.03	0.5 M $KHCO_3$	93	0.04	[14]
14	WSCAT	-0.86	0.1 M KCl (with KOH to pH=6.7)	98	N.A.	[8]
15	PCN-222(Fe)	-1.02	0.5 M $KHCO_3$	91	0.336	[42]
16	FePGH	-0.81	0.1 M $KHCO_3$	96.2	0.8	[43]
17	NiPor-CTF	-1.32	0.5 M $KHCO_3$	97	0.47	[44]

3.3. Mechanistic study

Further mechanistic analysis was performed to determine the role of covalent binding and elucidate the CO_2ERR mechanism. First of all, the influence of immobilization mode on the intrinsic activity of CoTAP was determined [45]. To achieve this, CO_2ERR was performed on CoTAP-cov and CoTAP-noncov electrodes containing progressively lower loadings of CoTAP [46]. In this regard, for CoTAP-noncov the surface concentration varied between 2×10^{-11} and 1×10^{-7} mol/cm^2. In turn, for CoTAP-cov the amount of CoTAP was scanned from 2×10^{-11} to 4×10^{-9} mol/cm^2. It should be noted that the maximum surface concentration for CoTAP-cov is set at 4×10^{-9} mol/cm^2 as beyond this value the CNTs amount will continue to rise and exceed the intended CNTs loading of ~120 μg/cm^2.

As expected, the TOFco gradually increases at the lower catalyst loadings for both CoTAP-cov and CoTAP-noncov. Indeed, for CoTAP-noncov the value of TOFco is 0.25 s^{-1} only at 1×10^{-7} mol/cm^2 (Fig. 7a, red trace). However, this raises to 5.8 s^{-1} for loadings below 4×10^{-11} mol/cm^2, indicating that all CoTAP molecules are active. Therefore, the TOF (ca. 5.8 s^{-1}) is regarded as an intrinsic TOF for CoTAP at −1.30 V in noncovalent immobilization mode. In contrast, the TOFco of CoTAP-cov shows a significantly more rapid growth from 6.0 s^{-1} at 4×10^{-9} mol/cm^2 to 36.6 s^{-1} at 2×10^{-11} mol/cm^2 where the activity reaches its intrinsic value (Fig. 7a, blue trace). The respective selectivities to CO are also invariably higher for CoTAP-cov which exhibits FEco of 9.8% at the lowest loading and ~100% upon saturation

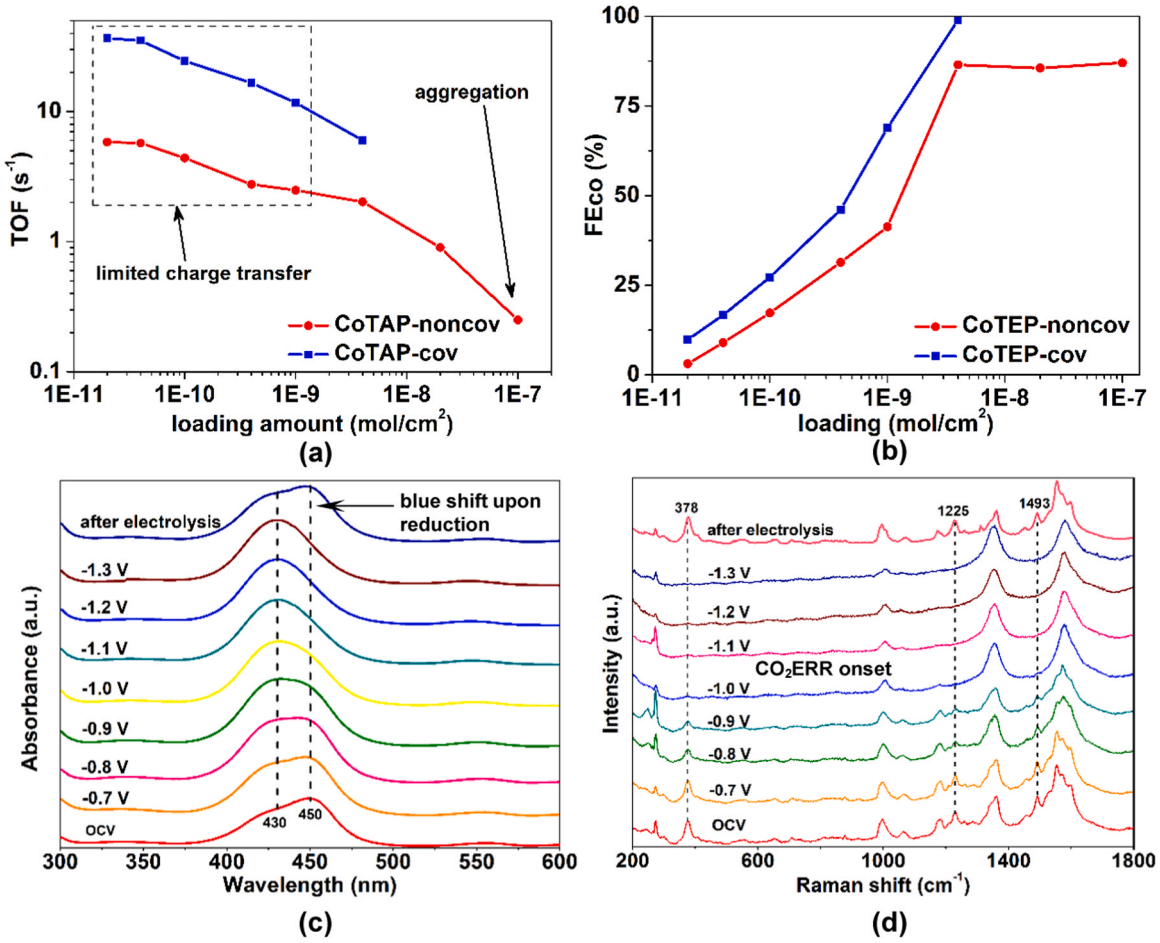

Fig. 7. (a) TOFco and (b) FEco observed for CoTAP-noncov and CoTAP-cov with various loading amounts after 60 min electrolysis at −1.30 V; (c) in-situ UV–vis and (d) in-situ Raman spectra of CoTAP-noncov (1×10^{-7} mol/cm^2) recorded under potentials ranging from open circuit voltage (OCV) to the potentials between −0.7 V and −1.3 V. (For interpretation of the references to colour in this figure legend, the reader is referred to the web version of this article.)

of the surface with CoTAP (Fig. 7b, blue trace). In turn, CoTAP-noncov shows FEco of 3.1% only at the lowest loading which rises steadily at first, but then levels off around 85% at the loading of 4×10^{-9} mol/cm^2 (Fig. 7b, red trace).

Next, in-situ spectroelectrochemical measurements were employed to elucidate the valence state of the catalyst and detect the presence of the long-lived reaction intermediates. For the UV–vis experiments, CoTAP was directly drop casted on the FTO glass and the spectra were recorded under potentials ranging from the open circuit voltage (OCV) to −1.3 V (Fig. 7c). The typical absorbance of CoTAP at OCV features a prominent Soret band at 450 nm and Q-band at 555 nm. Upon applying progressively negative potentials (−0.7 to −1.3 V vs Ag/AgCl) to the FTO/CoTAP electrode, both Soret and Q bands experience a blue shift to 430 nm and 542 nm, respectively. The wavelength drift indicates that more energy is required for the electron to be excited from the highest occupied molecular orbital to the empty anti-bonding orbital. This change could be attributed to the back donation [47] into the negatively charged porphyrin system of [Co^{I}TAP]$^{-}$. Furthermore, it is noted that the Soret band at 450 nm corresponding to uncharged Co^{II}TAP disappear completely upon transitioning into the potential where CO_2ERR takes place (below −1.0 V). Indeed, the spectrum of the electrode at − 0.9 V reveals a bimodal peak corresponding to a mixture of Co^{II}TPP and [Co^{I}TAP]$^{-}$. Thus, Co^{II}TAP species take no part in the reaction sequence, indicating that the entire catalytic cycle is driven only by [Co^{I}TAP]$^{-}$.

In-situ Raman spectra (Fig. 7d) were also recorded under negative potentials for CoTAP-noncov. A high surface loading of 1×10^{-7} mol/cm^2 was employed to assure a well-resolved Raman response. At OCV, the Raman spectrum clearly shows peaks at 378 cm^{-1}, 1225 cm^{-1} and 1493 cm^{-1} assigned to the stretching vibrations of the Co-N bond, the porphyrin scaffold, and the C_β-C_β bond, respectively. However, these peaks gradually disappear at more negative potentials as the forming species are Raman-silent due to the mismatch between the Q-band of the [Co^{I}TAP]$^{-}$ (542 nm) and the wavelength of the laser (633 nm). Also, no signals corresponding to the stretching vibrations of CO ligand or C═O group in Co-COOH intermediate were detected indicating that the reaction intermediates are short-lived.

The corresponding Tafel plots were derived for CoTAP-noncov and CoTAP-cov via plotting of the CO production current density against overpotential (Fig. 8). In this regard, CoTAP-noncov at a high loading (4×10^{-9} mol/cm^2) displays a slope of 289 mV/dec, which is consistent with the one for the same porphyrin catalyst reported by Lin et al. [38]. The value is far from the theoretical 118 mV/dec, indicating a strong interference of mass transport limitations. In contrast, CoTAP-noncov at a lower loading amount (4×10^{-11} mol/cm^2) displays a slope of 218 mV/dec, which is closer to the theoretical value, implying that the diffusion has been partially mitigated [45]. The lower value of the Tafel slope is most likely due to the improved dispersion of CoTAP on CNTs at a much lower surface concentration. Meanwhile, CoTAP-cov (4×10^{-9} mol/cm^2) exhibits a further decline of slope to 210 mV/dec similar to that of CoTAP-noncov (4×10^{-11} mol/cm^2) although the loading is higher by two orders of magnitude, which confirms that the dispersion of CoTAP on CNTs was improved by covalent immobilization.

These results allow one to deduce a reaction mechanism described in Fig. 9(a). First of all, a generally higher TOFco compared to

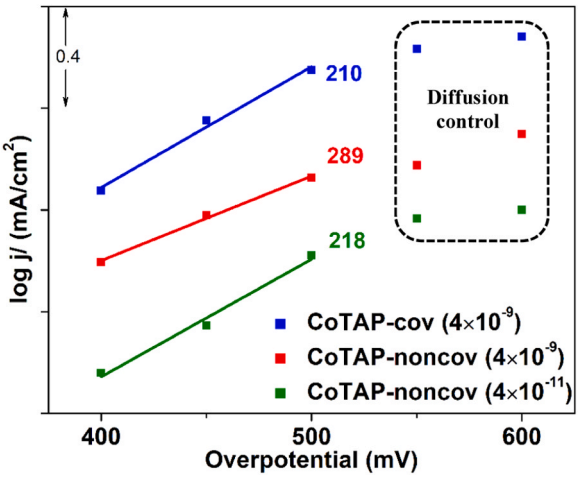

Fig. 8. Tafel plots observed on CoTAP-cov (4×10^{-9} mol/cm^2, blue trace), CoTAP-noncov (4×10^{-9} mol/cm^2, red trace) and CoTAP-noncov (4×10^{-11} mol/cm^2, green trace). (For interpretation of the references to colour in this figure legend, the reader is referred to the web version of this article.)

unsubstituted porphyrins most likely stems from a partial negative charge on the cobalt atom due to the resonance with -NH_2 groups [11]. The in-situ UV–vis and Raman spectra suggest that the catalyst resting state is [Co^{I}TAP]$^-$ as the Co^{II}TPP is not present on the surface during the CO_2ERR (Fig. 7c-d). The dependence of the reaction rate on the applied potential and a short lifetime of the intermediates correspond to the first electron transfer being a rate-determining step (RDS) [34].

The structure of the surface layer also exerts significant influence on the performance of the catalysts. Indeed, we noticed that any factor furnishing a more uniform porphyrin layer clearly favours the reaction kinetics. In this regard, Tafel slope declines for CoTAP-noncov at low loadings, but even at 4×10^{-11} mol/cm^2 CoTAP-noncov does not reach the performance of CoTAP-cov. Thus, the CO_2 transport towards CoTAP is significantly faster on CoTAP-cov due to the low thickness of the porphyrin film. This is evident at high loading of 2×10^{-8} mol/cm^2 where noncovalent immobilization results in severe aggregation (Fig. S4).

Furthermore, the intrinsic, diffusion-independent TOFco exhibited by CoTAP-cov is 6.3 times higher than that of CoTAP-noncov. Hence, the improved diffusion of CO_2 towards the active centres does not explain the enhanced activity by itself. In this regard, we recently demonstrated that the multimolecular layers of Co porphyrins feature extremely inhomogeneous charge transfer as the molecules located directly on the carbon surface feature faster electron delivery than those confined to the distant layers [42]. Thus, the direct covalent connection of CoTAP to the surface of CNT also boosts the overall reaction rate due to the faster electron migration (Fig. 9b). This feature, combined with the diffusion of CO_2 not being hindered by the layers of CoTAP makes CoTAP-cov one of the most active heterogeneous molecular catalysts to date. In turn, simple noncovalent immobilization results in aggregation and mismatch

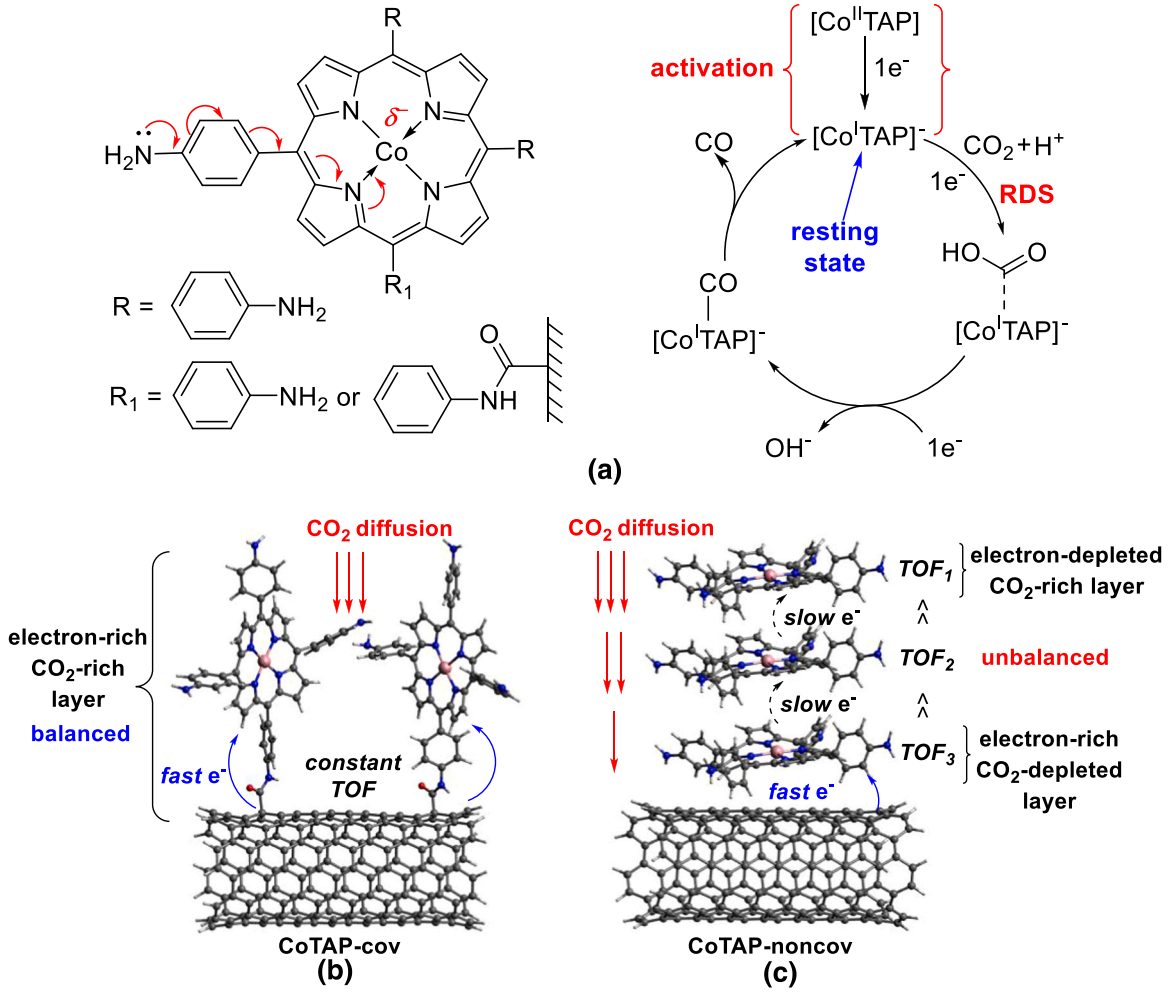

Fig. 9. The proposed mechanism of CO_2ERR reaction catalyzed by CoTAP (a) and dependence of TOF and electron transfer rates on the CoTAP immobilization mode for CoTAP-cov (b) and CoTAP-noncov (c).

between the inbound flux of CO_2 and outbound flux of electrons thus giving a material with inferior performance (Fig. 9c). Furthermore, the lower selectivity of noncovalently immobilized complex even beyond the point of surface saturation also most likely stems from the aggregation of CoTAP.

It is noted that CoTAP-cov has a higher TOF compared to CoTAP-noncov at various potentials. As illustrated in Fig. 9(b) and (c), noncovalent immobilization results in aggregation due to π-π stacking between porphyrins which slows down the CO_2 diffusion to the active sites and impairs the catalytic performance [48]. Hence, the introduction of covalent bond allows one to obtain a superb electrocatalyst for CO_2ERR while assuring efficient electron delivery and protecting the complex from severe aggregation.

4. Conclusions

In this work, the CO_2ERR electrocatalytic activity of amino-substituted Co porphyrin (CoTAP) was studied as a function of its immobilization mode on the surface of carbon nanotubes (CNTs). Over a wide potential range from −1.20 to − 1.40 V, the covalently grafted complex CoTAP-cov shows significantly higher TOFco and FEco compared to its noncovalent counterpart CoTAP-noncov. At −1.30 V (i.e. −1.095 V vs NHE), CoTAP-cov exhibits an excellent TOF of 6.0 s^{-1} and FEco of ~100% making it one of the best catalysts to date. Our experimental evidence suggests that the introduction of the donating -NH_2 group into the structure of porphyrin enhances the electron density on the cobalt center thus boosting its intrinsic activity to TOFco of 36.6 s^{-1}. We conclude that the amide bond acts as a molecular wire enhancing the electron transfer from CNTs to cobalt center. The Tafel analysis also reveals that the strong bond with the surface enhances the dispersion of CoTAP at high loadings and thus alleviates the mass transport limitations. Thus, covalent immobilization could actively promote CO_2ERR and has great potential in the rational design of electrocatalysts in the future.

CRediT authorship contribution statement

Shengshen Gu, Aleksei Marianov, Yijiao Jiang: Conceptualization, Supervision, Writing – review & editing. **Shengshen Gu:** Data curation, Formal analysis, Investigation, Methodology, Writing – original draft.

Declaration of Competing Interest

The authors declare that they have no known competing financial interests or personal relationships that could have appeared to influence the work reported in this paper.

Acknowledgement

Financial support from the ARC Discovery Project (DP1901013720) and the Chinese Scholarship Council (CSC) is gratefully acknowledged. The authors thank the technical support from the Macquarie Analytical and Fabrication Facility.

Appendix A. Supporting information

Supplementary data associated with this article can be found in the online version at doi:10.1016/j.apcatb.2021.120750.

References

[1] H. Shin, K.U. Hansen, F. Jiao, Techno-economic assessment of low-temperature carbon dioxide electrolysis, Nat. Sustain. (2021).
[2] K.P. Kuhl, E.R. Cave, D.N. Abram, T.F. Jaramillo, New insights into the electrochemical reduction of carbon dioxide on metallic copper surfaces, Energy Environ. Sci. 5 (5) (2012) 7050–7059.
[3] K.P. Kuhl, T. Hatsukade, E.R. Cave, D.N. Abram, J. Kibsgaard, T.F. Jaramillo, Electrocatalytic conversion of carbon dioxide to methane and methanol on transition metal surfaces, J. Am. Chem. Soc. 136 (40) (2014) 14107–14113.
[4] Y.H. Chen, C.W. Li, M.W. Kanan, Aqueous CO_2 reduction at very low overpotential on oxide-derived Au nanoparticles, J. Am. Chem. Soc. 134 (49) (2012) 19969–19972.
[5] X.Y. Lu, T.H. Tan, Y.H. Ng, R. Amal, Highly selective and stable reduction of CO_2 to CO by a graphitic carbon nitride/carbon nanotube composite electrocatalyst, Chem. Eur. J. 22 (34) (2016) 11991–11996.
[6] J.J. Wu, R.M. Yadav, M.J. Liu, P.P. Sharma, C.S. Tiwary, L.L. Ma, X.L. Zou, X. D. Zhou, B.I. Yakobson, J. Lou, P.M. Ajayan, Achieving highly efficient, selective, and stable CO_2 reduction on nitrogen-doped carbon nanotubes, ACS Nano 9 (5) (2015) 5364–5371.
[7] E.E. Benson, C.P. Kubiak, A.J. Sathrum, J.M. Smieja, Electrocatalytic and homogeneous approaches to conversion of CO_2 to liquid fuels, Chem. Soc. Rev. 38 (1) (2009) 89–99.
[8] C. Costentin, M. Robert, J.M. Saveant, A. Tatin, Efficient and selective molecular catalyst for the CO_2-to-CO electrochemical conversion in water, Proc. Nat. Acad. Sci. U.S.A. 112 (22) (2015) 6882–6886.
[9] C. Costentin, S. Drouet, M. Robert, J.M. Saveant, A local proton source enhances CO_2 electroreduction to CO by a molecular Fe catalyst, Science 338 (6103) (2012) 90–94.
[10] M.E. Dry, The Fischer-Tropsch process: 1950-2000, Catal. Today 71 (3–4) (2002) 227–241.
[11] M.H. Zhu, D.T. Yang, R.Q. Ye, J. Zeng, N. Corbin, K. Manthiram, Inductive and electrostatic effects on cobalt porphyrins for heterogeneous electrocatalytic carbon dioxide reduction, Catal. Sci. Technol. 9 (4) (2019) 974–980.
[12] M. Abdinejad, A. Seifitokaldani, C. Dao, E.H. Sargent, X.-A. Zhang, H.B. Kraatz, Enhanced electrochemical reduction of CO_2 catalyzed by cobalt and iron amino porphyrin complexes, ACS Appl. Energy Mater. 2 (2) (2019) 1330–1335.
[13] D. Tasis, N. Tagmatarchis, A. Bianco, M. Prato, Chemistry of carbon nanotubes, Chem. Rev. 106 (3) (2006) 1105–1136.
[14] A. Maurin, M. Robert, Noncovalent immobilization of a molecular iron-based electrocatalyst on carbon electrodes for selective, efficient CO_2-to-CO conversion in water, J. Am. Chem. Soc. 138 (8) (2016) 2492–2495.
[15] S. Aoi, K. Mase, K. Ohkubo, S. Fukuzumi, Selective electrochemical reduction of CO_2 to CO with a cobalt chlorin complex adsorbed on multi-walled carbon nanotubes in water, Chem. Commun. 51 (50) (2015) 10226–10228.
[16] L. Sun, V. Reddu, A.C. Fisher, X. Wang, Electrocatalytic reduction of carbon dioxide: opportunities with heterogeneous molecular catalysts, Energy Environ. Sci. 13 (2) (2020) 374–403.
[17] T. Atoguchi, A. Aramata, A. Kazusaka, M. Enyo, Cobalt(II) tetraphenylporphyrin pyridine complex fixed on a glassy-carbon electrode and its prominent catalytic activity for reduction of carbon-dioxide, J. Chem. Soc. Chem. Comm. 3 (1991) 156–157.
[18] T. Atoguchi, A. Aramata, A. Kazusaka, M. Enyo, Electrocatalytic activity of coiitpp-pyridine complex modified carbon electrode for CO_2 reduction, J. Electroanal. Chem. 318 (1–2) (1991) 309–320.
[19] H. Aga, A. Aramata, Y. Hisaeda, The electroreduction of carbon dioxide by macrocyclic cobalt complexes chemically modified on a glassy carbon electrode, J. Electroanal. Chem. 437 (1–2) (1997) 111–118.
[20] S. Gu, A.N. Marianov, Y. Zhu, Y. Jiang, Cobalt porphyrin immobilized on the TiO_2 nanotube electrode for CO_2 electroreduction in aqueous solution, J. Energy Chem. 55 (2021) 219–227.
[21] X.M. Hu, Z. Salmi, M. Lillethorup, E.B. Pedersen, M. Robert, S.U. Pedersen, T. Skrydstrup, K. Daasbjerg, Controlled electropolymerisation of a carbazole-functionalised iron porphyrin electrocatalyst for CO_2 reduction, Chem. Comm. 52 (34) (2016) 5864–5867.
[22] M. Wang, L.J. Chen, T.C. Lau, M. Robert, A hybrid Co quaterpyridine complex/carbon nanotube catalytic material for CO_2 reduction in water, Angew. Chem. Int. Ed. 57 (26) (2018) 7769–7773.
[23] W.W. Kramer, C.C.L. McCrory, Polymer coordination promotes selective CO_2 reduction by cobalt phthalocyanine, Chem. Sci. 7 (4) (2016) 2506–2515.
[24] A.N. Marianov, Y.J. Jiang, Covalent ligation of Co molecular catalyst to carbon cloth for efficient electroreduction of CO_2 in water, Appl. Catal. B: Environ. 244 (2019) 881–888.
[25] J. Su, J.-J. Zhang, J. Chen, Y. Song, L. Huang, M. Zhu, B.I. Yakobson, B.Z. Tang, R. Ye, Building a stable cationic molecule/electrode interface for highly efficient and durable CO_2 reduction at an industrially relevant current, Energy Environ. Sci. 14 (1) (2021) 483–492.
[26] G. Prabhavathi, R. Yamuna, A.C. Jafer, Covalent functionalization and solubilization of multi-walled carbon nanotubes by using zinc and copper complexes of meso-tetra(4-aminophenyl) porphyrin, J. Organometall. Chem. 861 (2018) 219–229.
[27] A. Wang, J. Song, Z. Huang, Y. Song, W. Yu, H. Dong, W. Hu, M.P. Cifuentes, M. G. Humphrey, L. Zhang, J. Shao, C. Zhang, Multi-walled carbon nanotubes covalently functionalized by axially coordinated metal-porphyrins: facile syntheses and temporally dependent optical performance, Nano Res. 9 (2) (2016) 458–472.
[28] J.L. Bahr, J. Yang, D.V. Kosynkin, M.J. Bronikowski, R.E. Smalley, J.M. Tour, Functionalization of carbon nanotubes by electrochemical reduction of aryl diazonium salts: a bucky paper electrode, J. Am. Chem. Soc. 123 (27) (2001) 6536–6542.
[29] G. Prabhavathi, M. Arjun, R. Yamuna, Synthesis, characterization and photoluminescence properties of tetra(aminophenyl) porphyrin covalently linked to multi-walled carbon nanotubes, J. Chem. Sci. 129 (6) (2017) 699–706.

[30] D.R. Roy, E.V. Shah, S. Mondal Roy, Optical activity of Co-porphyrin in the light of IR and Raman spectroscopy: a critical DFT investigation, Spectrochim. Acta A Mol. Biomol. Spectrosc. 190 (2018) 121–128.
[31] K.S. Lokesh, M. De Keersmaecker, A. Adriaens, Self sssembled films of porphyrins with amine groups at different positions: influence of their orientation on the corrosion inhibition and the electrocatalytic activity, Molecules 17 (7) (2012) 7824–7842.
[32] H.K. Hall, C.H. Lueck, The ionization mechanism for the hydrolysis of acyl chlorides, J. Org. Chem. 28 (10) (1963) 2818–2825.
[33] X.-M. Hu, M.H. Rønne, S.U. Pedersen, T. Skrydstrup, K. Daasbjerg, Enhanced catalytic activity of cobalt porphyrin in CO_2 electroreduction upon immobilization on carbon materials, Angew. Chem. Int. Ed. 56 (23) (2017) 6468–6472.
[34] A.N. Marianov, A.S. Kochubei, T. Roman, O.J. Conquest, C. Stampfl, Y. Jiang, Resolving deactivation pathways of Co porphyrin-based electrocatalysts for CO_2 reduction in aqueous medium, ACS Catal. 11 (6) (2021) 3715–3729.
[35] Soustelle, M. In An Introduction to Chemical Kinetics, 2011; pp 43–71.
[36] G.O. Larrazábal, M. Ma, B. Seger, A comprehensive approach to investigate CO_2 reduction electrocatalysts at high current densities, Acc. Mater. Res. 2 (4) (2021) 220–229.
[37] M.H. Zhu, J.C. Chen, L.B. Huang, R.Q. Ye, J. Xu, Y.F. Han, Covalently grafting cobalt porphyrin onto carbon nanotubes for efficient CO_2 electroreduction, Angew. Chem. Int. Ed. 58 (20) (2019) 6595–6599.
[38] S. Lin, C.S. Diercks, Y.-B. Zhang, N. Kornienko, E.M. Nichols, Y. Zhao, A.R. Paris, D. Kim, P. Yang, O.M. Yaghi, C.J. Chang, Covalent organic frameworks comprising cobalt porphyrins for catalytic CO_2 reduction in water, Science 349 (6253) (2015) 1208–1213.
[39] T. Wang, L. Xu, Z. Chen, L. Guo, Y. Zhang, R. Li, T. Peng, Central site regulation of cobalt porphyrin conjugated polymer to give highly active and selective CO_2 reduction to CO in aqueous solution, Appl. Catal. B: Environ. 291 (2021), 120128.
[40] Y. Lu, J. Zhang, W. Wei, D.-D. Ma, X.-T. Wu, Q.-L. Zhu, Efficient carbon dioxide electroreduction over ultrathin covalent organic framework nanolayers with isolated cobalt porphyrin units, ACS Appl. Mater. Interfaces 12 (34) (2020) 37986–37992.
[41] A. Maurin, M. Robert, Catalytic CO_2-to-CO conversion in water by covalently functionalized carbon nanotubes with a molecular iron catalyst, Chem. Comm. 52 (81) (2016) 12084–12087.
[42] B.-X. Dong, S.-L. Qian, F.-Y. Bu, Y.-C. Wu, L.-G. Feng, Y.-L. Teng, W.-L. Liu, Z.-W. Li, Electrochemical reduction of CO_2 to CO by a heterogeneous catalyst of Fe–porphyrin-based metal–organic framework, ACS Appl. Energy Mater. 1 (9) (2018) 4662–4669.
[43] J. Choi, J. Kim, P. Wagner, S. Gambhir, R. Jalili, S. Byun, S. Sayyar, Y.M. Lee, D. R. MacFarlane, G.G. Wallace, D.L. Officer, Energy efficient electrochemical reduction of CO_2 to CO using a three-dimensional porphyrin/graphene hydrogel, Energy Environ. Sci. 12 (2) (2019) 747–755.
[44] C. Lu, J. Yang, S. Wei, S. Bi, Y. Xia, M. Chen, Y. Hou, M. Qiu, C. Yuan, Y. Su, F. Zhang, H. Liang, X. Zhuang, Atomic Ni anchored covalent triazine framework as high efficient electrocatalyst for carbon dioxide conversion, Adv. Funct. Mater. 29 (10) (2019), 1806884.
[45] M.H. Zhu, J.C. Chen, R. Guo, J. Xu, X.C. Fang, Y.F. Han, Cobalt phthalocyanine coordinated to pyridine-functionalized carbon nanotubes with enhanced CO_2 electroreduction, Appl. Catal. B-Environ. 251 (2019) 112–118.
[46] M.H. Zhu, R.Q. Ye, K. Jin, N. Lazouski, K. Manthiram, Elucidating the reactivity and mechanism of CO_2 electroreduction at highly dispersed cobalt phthalocyanine, ACS Energy Lett. 3 (6) (2018) 1381–1386.
[47] D. Behar, T. Dhanasekaran, P. Neta, C.M. Hosten, D. Ejeh, P. Hambright, E. Fujita, Cobalt porphyrin catalyzed reduction of CO_2. Radiation chemical, photochemical, and electrochemical studies, J. Phys. Chem. A 102 (17) (1998) 2870–2877.
[48] A.N. Marianov, A.S. Kochubei, T. Roman, O.J. Conquest, C. Stampfl, Y. Jiang, Modeling and experimental study of the electron transfer kinetics for non-ideal electrodes using variable-frequency square wave voltammetry, Anal. Chem. 93 (29) (2021) 10175–10186.